

Organic single-crystal complementary inverter

Alejandro L. Briseno

Department of Chemistry and Biochemistry and Exotic Materials Institute, University of California–Los Angeles, Los Angeles, California 90095

Ricky J. Tseng, Sheng-Han Li, Chih-Wei Chu, and Yang Yang^{a)}

Department of Materials Science and Engineering, University of California–Los Angeles, Los Angeles, California 90095

Eduardo H. L. Falcao and Fred Wudl^{b)}

Department of Chemistry and Biochemistry and Exotic Materials Institute, University of California–Los Angeles, Los Angeles, California 90095

Mang-Mang Ling, Hong Zheng Chen, and Zhenan Bao^{c)}

Department of Chemical Engineering, Stanford University, Stanford, California 94305

Hong Meng

DuPont Experimental Station, Wilmington, Delaware 19880

Christian Kloc

Bell Laboratories, Lucent Technologies, 600 Mountain Ave., Murray Hill, New Jersey 07974

(Received 16 July 2006; accepted 5 October 2006; published online 29 November 2006)

The authors demonstrate the operation of an organic single-crystal complementary circuit in the form of a simple inverter. The device is constructed from a high mobility *p*-type organic single-crystal transistor of tetramethylpentacene (TMPC) and a *n*-type single-crystal transistor of *N,N'*-di[2,4-difluorophenyl]-3,4,9,10-perylenetetracarboxylic diimide (PTCDI). Field-effect mobilities of up to 1.0 cm²/V s are reported for TMPC devices, while a mobility of 0.006 cm²/V s is reported for a *n*-type PTCDI single-crystal device. Considering that organic single-crystal inverters have not yet been explored, they are representative of potential candidates for use in high-performance complementary circuits. © 2006 American Institute of Physics.

[DOI: 10.1063/1.2390646]

An inverter is considered to be the most basic circuit element in complementary metal-oxide semiconductor technology. Complementary inverters consisting of both *p*- and *n*-channel devices are reported to have advantages over homogeneous-structured devices (i.e., either *p*- or *n*-channel only).¹ These advantages include improved noise margins, lower power dissipation, and device stability.^{1,2} It has been demonstrated that these particular advantages also apply to organic thin film circuits such as ring oscillators, shift registers, flip-flop circuits, and inverters.^{1–7} An interesting note is that most of the work to date has focused on organic polycrystalline thin film circuits only, and thus far, little or no work has been demonstrated with organic single crystals. Organic single crystals are of interest, because they exhibit excellent charge transport in field-effect transistors.^{8–10} Here we demonstrate that organic single-crystal complementary inverters can be fabricated and yield excellent electrical characteristics. We employ tetramethylpentacene¹¹ (TMPC) and *N,N'*-di[2,4-difluorophenyl]-3,4,9,10-perylenetetracarboxylic diimide (PTCDI) as *p*-type and *n*-type¹² organic semiconductors, respectively. Neither of these materials has been investigated in their single-crystal forms. *p*-type field-effect mobilities of 1 cm²/V s and *n*-type field-effect mobilities of 0.006 cm²/V s are reported for TMPC and PTCDI, respectively. By electrically combining a *p*-type TMPC device and

n-type PTCDI device, we demonstrate the operation of an organic single-crystal complementary inverter.

The fabrication of single-crystal transistors begins from the growth of crystals by horizontal physical vapor transport growth.¹³ Single crystals were grown in a stream of argon at a flow rate of ~100 ml/min and growth times ranging from 4 to 16 h. TMPC single crystals were typically thin, flat flakes usually 3 × 3 mm² in size with thicknesses ranging from 400 nm to 2 μm. PTCDI crystals were typically 0.5 × 2 mm² in size and usually about 1–3 μm thick. Single-crystal transistors were fabricated on highly doped Si containing 300 nm SiO₂ dielectric. The source-drain electrodes were thermally evaporated with 5 nm Cr and 50 nm Au under a vacuum of ~1 × 10⁻⁵ torr. A solution of 10 mM 4-nitrobenzenethiol (Aldrich) in dry toluene was used to modify source-drain electrodes for *p*-type single-crystal devices only (devices were placed in the thiol solution for 2 h and carefully rinsed with toluene). It has been reported that this type of surface modification on gold electrodes can improve device performance by increasing carrier densities of holes at the metal/semiconductor interface for *p*-type semiconductor devices.¹⁴ Organic single crystals were carefully picked with a Teflon-coated tweezers and electrostatically bonded across source-drain electrodes (bottom-contact configuration). This flip-crystal technique¹⁵ is widely used to fabricate single-crystal transistors for field-effect studies. Figures 1(a) and 1(b) show the chemical structures and optical images of the organic semiconductors. TMPC and PTCDI are utilized as *p*-type and *n*-type materials, respec-

^{a)}Electronic mail: yangy@ucla.edu

^{b)}Electronic mail: wudl@chem.ucla.edu

^{c)}Electronic mail: zbao@chemeng.stanford.edu

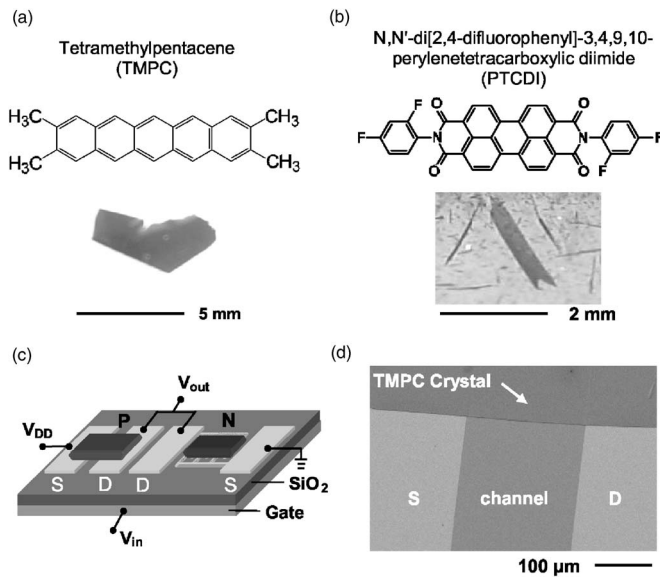


FIG. 1. Chemical structures and optical micrographs of (a) tetramethylpentacene and (b) N,N' -di[2,4-difluorophenyl]-3,4,9,10-perylenetetracarboxylic diimide. (c) A schematic complementary inverter circuit devised from a p -type TMPC and a n -type PTCDI transistor. (d) A SEM image of a TMPC crystal electrostatically bonded across source-drain electrodes.

tively. The organic single-crystal inverter device configuration is shown in Fig. 1(c).

The scanning electron microscope (SEM) images were obtained with a JEOL JSM 6700F electron microscope. Samples were coated with ~ 5 nm of gold prior to SEM imaging. Electrical measurements were performed using an HP 4155B semiconductor parameter analyzer. Single-crystal thicknesses were measured with a profilometer (Dektak 3030) and the SEM instrument. The crystal thicknesses used in fabricating the transistors were 400–1200 nm for TMPC and 1500 nm for PTCDI. An actual TMPC single-crystal device is shown in Fig. 1(d). The SEM image clearly shows a flat crystal across the source-drain electrodes and the channel region. From the SEM image, the estimated crystal thickness is about 400 nm and the crystal appears to have good electrostatic adhesion to the underlying dielectric and electrode surface. The good adhesion along the surface of the channel provides effective carrier transport along the crystal/dielectric interface.

All measurements on TMPC single-crystal devices were made in normal room atmosphere with a standard probe station. For PTCDI devices, we found that the device characteristics were improved when measured under vacuum. For example, we observed a negative shift in threshold voltage from ~ 14 V (air) to 8.3 V (vacuum), an increase in current on/off ratio from ~ 45 to 120, and finally the onset of the output characteristics was much improved and well resolved under vacuum. We found no measurable distinction in field-effect mobility in devices measured under vacuum. Therefore, the results reported for n -channel devices are measured in vacuum ($\sim 10^{-5}$ torr). Due to the low mobility of the n -channel material compared to the p -channel material, interdigitated electrodes were implemented to yield characteristics with higher output currents. The channel width/length (W/L) for our devices was carefully examined from the microscope based on the crystal cover area across the channels ($W/L=14$ for TMPC and $W/L=140$ for PTCDI). The field-

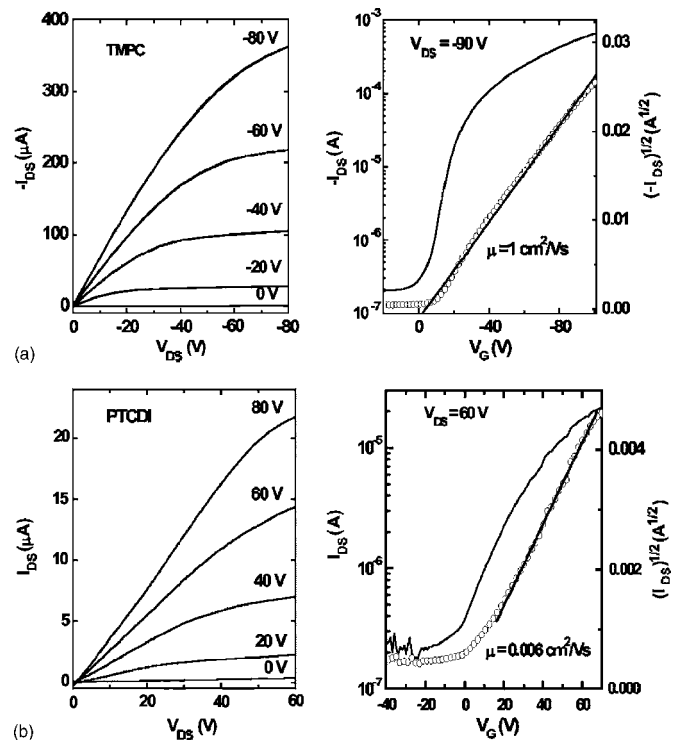


FIG. 2. Electrical characteristics of (a) TMPC and (b) PTCDI devices, exhibiting field-effect mobilities of 1.0 and 0.006 $\text{cm}^2/\text{V s}$, respectively. The left panel shows the output current (V_{DS} vs I_{DS}), and the right panel shows the transfer curves ($I_{DS}^{1/2}$ vs V_G).

effect mobility was calculated from the saturation region using equation of $I_{DS} = (WC\mu/2L)(V_G - V_T)^2$, where the capacitance $C = 10$ nF/cm² for 300 nm thick SiO₂ gate dielectric and V_T is the threshold voltage. The subthreshold slopes were calculated from the equation $S = dV_G/d(\log I_{DS})$.¹⁶

Figure 2 shows the I_{DS} - V_{DS} characteristics (left panel) while the right panel shows both the $(I_{DS})^{0.5}$ - V_G and $\log(I_{DS})$ - V_G characteristics for typical p -type TMPC [Fig. 2(a)] and n -type PTCDI single-crystal device [Fig. 2(b)]. The I_{DS} - V_{DS} curves show well-defined transistor characteristics with saturation effects at $V_G > -20$ V and $V_{DS} > -40$ V for a TMPC device. We extracted a field-effect mobility of 1.03 $\text{cm}^2/\text{V s}$ in the saturation region at $V_{DS} = -90$ V, on/off ratio of $\sim 10^4$, threshold voltage of -3 V, and a subthreshold swing of 7.2 V nF/decade cm². Previously, we reported TMPC thin film transistors with mobilities as high as 0.3 $\text{cm}^2/\text{V s}$ and on/off ratios on the order of 10^3 .¹¹ Our results herein exhibit more than a threefold increase in field-effect mobility. This may indicate that single-crystal devices fabricated from pentacene derivatives may potentially show greater performances compared to thin film counterparts, and thus give rise to opportunities with materials that do not yield impressive mobilities in thin film devices. For the PTCDI single-crystal transistor, we determined a field-effect mobility of 0.006 $\text{cm}^2/\text{V s}$ at $V_{DS} = 60$ V. The on/off ratio is ~ 120 , threshold voltage of 8.3 V, and a subthreshold swing of 24 V nF/decade cm² is observed. We further examined the gate dependence of these single-crystal transistors. From Fig. 3(a), the electrical characteristics reveal that single-crystal devices show a nearly no gate dependence beyond -30 V for TMPC when mobility is plotted versus the absolute gate voltage $|V_G|$. The same plot also shows that the PTCDI device exhibits a fairly weak gate dependence in gate

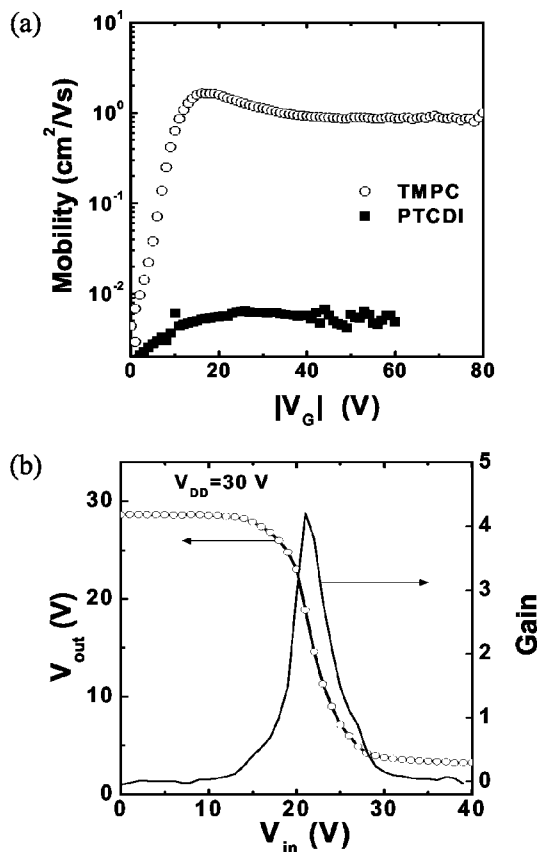


FIG. 3. (a) Plot of mobility as a function of gate voltages for TMPC and PTCDI devices. The data were calculated from the given equation $\mu = (2L/WCi)(\partial I_{DS}^{1/2}/\partial V_G)^2$. (b) The inverter and gain characteristics acquired from TMPC and PTCDI transistors. The supply voltage is $V_{DD}=30$ V.

voltages beyond 20 V. Therefore, these results show that gate dependence does not seem to occur in our electrostatically bonded single-crystal devices. This evidence coincides with previous work showing that gate voltage dependence is a more prevalent phenomenon commonly observed with traps at grain boundaries in polycrystalline thin film transistors¹⁷ as opposed to single-crystal devices. We note, however, that single-crystal transistors have been reported to exhibit weak gate voltage dependency.¹⁸

In Fig. 3(b), we demonstrate a complementary inverter circuit devised from a *p*-type (TMPC) and a *n*-type (PTCDI) device. We point out that the inverter devices were measured in room atmosphere and not under vacuum. The graph shows how the *p*-channel load turns off as the *n*-channel driver sharply turns on as the input voltage is gradually increased. Despite the fact that there is a large mismatch in charge carrier mobilities between the two semiconducting materials, a well-defined transfer curve can still be observed. It is obvious that the initial output voltage (~ 28 V) is slightly lower than the supply voltage (30 V) at zero input voltage (V_{in}). It may be possible that these nonideal characteristics arise from leakage currents, but more likely ascribed to the aforementioned incongruity in the mobilities of *n*- and *p*-channel devices. Nevertheless, we report a gain of 4.2 for our inverter device, comparable with literature reports.³ We believe that it may be possible to achieve larger gain values by utilization of a higher mobility *n*-channel material.¹²

In conclusion, we report field-effect mobilities as high as $1 \text{ cm}^2/\text{V s}$ for TMPC and $0.006 \text{ cm}^2/\text{V s}$ for PTCDI single-crystal transistors. TMPC single-crystal devices show a threefold increase in mobility over previously reported TMPC thin film devices.¹¹ We also demonstrated an all organic single-crystal complementary inverter. More research on the implementation of organic single-crystal complementary inverters is ongoing in order to achieve higher circuit performances. In addition, we are also pursuing the patterning of organic single-crystal complementary circuits on flexible substrates⁹ for applications in displays and wearable electronics.

One of the authors (A.L.B.) acknowledges the Bell Labs Graduate Research Fellowship. Authors A.L.B., F.W., R.J.T., and Y.Y. acknowledge financial support from the Air Force Office of Scientific Research (AFOSR Grant No. F49620-03-1-0101). Another author (Z.B.) acknowledges partial support from the Stanford Center for Polymeric Interfaces and Macromolecular Assemblies (NSF-Center MRSEC under Award No. DMR-0213618) and the Stanford School of Engineering. They also thank Qian Miao for stimulating discussions and helpful remarks.

¹B. Crone and A. Dodabalapur, in *Printed Organic and Molecular Electronics*, edited by D. R. Gamota, P. Brazis, K. Kalyanasundaram, and J. Zhang (Kluwer Academic, Boston), Chap. 4.3, p. 493.

²E. J. Meijer, D. M. De Leeuw, S. Setayesh, E. Van Veenendaal, B.-H. Huisman, P. W. M. Blom, J. C. Hummelen, U. Scherf, and T. M. Klapwijk, *Nat. Mater.* **2**, 678 (2003).

³B. K. Crone, A. Dodabalapur, R. Sarpeshkar, R. W. Filas, Y.-Y. Lin, Z. Bao, J. H. O'Neill, W. Li, and H. E. Katz, *J. Appl. Phys.* **89**, 5125 (2001).

⁴S. De Vusser, S. Steudel, K. Myny, J. Genoe, and P. Heremans, *Appl. Phys. Lett.* **88**, 162116 (2006).

⁵B. Crone, A. Dodabalapur, Y. Y. Lin, R. W. Filas, Z. Bao, R. Sarpeshkar, H. E. Katz, and W. Li, *Nature (London)* **403**, 521 (2000).

⁶G. H. Gelinck, H. E. A. Huitema, E. V. Veenendaal, E. Cantatore, L. Schrijnemakers, J. B. P. H. Van Der Putten, T. C. T. Geuns, M. Beenhackers, J. B. Giesbers, B. H. Huisman, E. J. Meijer, E. M. Benito, F. J. Touwslager, A. W. Marsman, B. J. E. Van Rens, and D. M. De Leeuw, *Nat. Mater.* **3**, 106 (2004).

⁷C. Rost, D. J. Gundlach, S. Karg, and W. Rieß, *J. Appl. Phys.* **95**, 5782 (2004).

⁸V. C. Sundar, J. Zaumseil, V. Podzorov, E. Menard, R. L. Willett, T. Someya, M. E. Gershenson, and J. A. Rogers, *Science* **303**, 1644 (2004).

⁹A. L. Briseno, R. J. Tseng, M. M. Ling, E. H. L. Falco, Y. Yang, F. Wudl, and Z. Bao, *Adv. Mater. (Weinheim, Ger.)* **18**, 2320 (2006).

¹⁰R. W. I. de Boer, M. E. Gershenson, A. F. Morpurgo, and V. Podzorov, *Phys. Status Solidi A* **201**, 1302 (2004).

¹¹H. Meng, M. Bendikov, G. Mitchell, R. Helgeson, F. Wudl, Z. Bao, T. Siegrist, Ch. Kloc, and C.-H. Chen, *Adv. Mater. (Weinheim, Ger.)* **15**, 1090 (2003).

¹²P. R. L. Malenfant, C. D. Dimitrakopoulos, J. D. Gelorme, L. L. Kosbar, and T. O. Graham, *Appl. Phys. Lett.* **80**, 2517 (2002).

¹³R. A. Laudise, Ch. Kloc, P. G. Simpkins, and T. Siegrist, *J. Cryst. Growth* **187**, 449 (1998).

¹⁴D. J. Gundlach, L. Jia, and T. N. Jackson, *IEEE Electron Device Lett.* **22**, 571 (2001).

¹⁵C. Goldmann, S. Haas, C. Krellner, K. P. Pernstich, D. J. Gundlach, and B. Batlogg, *J. Appl. Phys.* **96**, 2080 (2004).

¹⁶V. Podzorov, S. E. Sysoev, E. Loginova, V. M. Pudalov, and M. E. Gershenson, *Appl. Phys. Lett.* **83**, 3504 (2003).

¹⁷G. Horowitz, M. E. Hajlaoui, and R. Hajlaoui, *J. Appl. Phys.* **87**, 4456 (2000).

¹⁸R. Zeis, C. Besnard, T. Siegrist, C. Schlockermann, X. Chi, and Ch. Kloc, *Chem. Mater.* **18**, 244 (2006).